Computers and Geotechnics 134 (2021) 104091

Contents lists available at ScienceDirect

Computers and Geotechnics

journal homepage: www.elsevier.com/locate/compgeo

Research Paper

Unsaturated thermal consolidation around a heat source

Davood Yazdani Cherati [a,1], Omid Ghasemi-Fare [b,2,*]

[a] Sharif University of Technology, Iran
[b] University of Louisville, United States

ARTICLE INFO

Keywords:
Unsaturated thermal consolidation
Unsaturated soils
THM analysis
Analytical solution
Fourier-Laplace transformation
Green's function theory

ABSTRACT

Thermal loadings in saturated (two-phase) clays induce excess pore water pressure due to the difference in the thermal expansion coefficient of the pore volume and the pore water. The gradual dissipation of the excess pore water pressure causes thermal volume reduction which is known as thermal consolidation. However, thermal consolidation in a three-phase soil system such as unsaturated soil is more sophisticated. In this paper, an analytical model for thermal consolidation around a heat source embedded in unsaturated clay or in calyey soils containing two immiscible fluids is developed based on the effective stress concept. Governing equations, including energy, mass, and momentum balance equations are developed. Coexisting solid and pore fluids are assumed to be in local thermal equilibrium. First, a solution is provided using Fourier-Laplace transformation by considering constant coefficients. The inverse transformation is carried out fully analytically and thus, a closed-form solution is proposed. Then, the variations of soil properties during the thermal consolidation process are considered through a temporal discretization process. The developed model is validated using Green's function theory and the equations and results are compared with the available models in the literature. Results indicate the capability of the model to accurately predict thermal consolidation in a three-phase clayey soil.

1. Introduction

Predicting the thermo-hydro-mechanical (THM) response of porous media is of cardinal importance in various engineering problems, including deep waste disposal (Gibb, 2000), harvesting shallow (Cherati and Ghasemi-Fare, 2019; Cherati et al., 2020; Senejani et al., 2020) and deep (Hirschberg et al., 2014; Falcone et al., 2018) geothermal energy, deep drilling, and excavation (Abousleiman and Ekbote, 2005; Tao and Ghassemi, 2010), oil extraction (Kiamanesh, 1992; Pan et al., 2005), fire resistance of concrete (Khoury, 2000; Kodur and Dwaikat, 2008), buried electrical cables (Abdel-Hadi and Mitchell, 1981; de Lieto Vollaro et al., 2011), and stability of road subgrades subjected to temperature fluctuations (Asefzadeh, 2019; Teltayev and Suppes, 2019).

Thermal stresses create volume expansion in both pore fluid and solid soils. However, due to the difference in thermal expansion coefficients of the pore volume and pore fluid, excess pore fluid pressure will be induced (Ghasemi-Fare and Basu, 2016; Tamizdoust and Ghasemi-Fare, 2020a). Generation of the excess pore water pressure reduces effective stress, weakens the soil, and may result in soil thermal failure (Song et al., 2018). In addition, the dissipation of excess pore fluid pressure causes soil thermal volume reduction (thermal consolidation) in normally consolidated (NC) clays (Joshaghani and Ghasemi-Fare, 2019). Thermal consolidation in a three-phase soil (e.g., unsaturated clay) is more sophisticated since it requires solving a set of governing equations that couple more unknown variables. Several experimental analyses have been performed to study the thermal consolidation in fine-grained soils and investigate alterations in soil mechanical properties during thermal loadings (Abuel-Naga et al., 2006; Uchaipichat and Khalili, 2009; Coccia and McCartney, 2016). However, in small scale experimental modeling (temperature-controlled condition), the temperature of the whole medium changes almost equally, and thus the effects of temporal and special variation of thermal stress cannot be observed accurately. This is while, a heat source buried in the ground generates transient heat flow in the soil medium.

Many analytical and numerical models were developed to address soil consolidation induced by transient thermal loads (Yazdani Cherati and Ghasemi-Fare, 2021) based on Biot's consolidation theory (Biot, 1941). Equations governing thermal consolidation are strongly coupled; however, researchers mostly consider energy conservation equation

* Corresponding author.
E-mail addresses: Davood.Yazdani71@student.sharif.edu (D.Y. Cherati), omid.ghasemifare@louisville.edu (O. Ghasemi-Fare).
[1] Postal address: Department of Civil and Environmental Engineering, Sharif University of Technology, Azadi Ave, Tehran, Iran.
[2] Postal address: 132 Eastern Pkwy, Department of Civil and Environmental Engineering, University of Louisville, Louisville, KY 40207, United States.

https://doi.org/10.1016/j.compgeo.2021.104091
Received 16 September 2020; Received in revised form 31 January 2021; Accepted 18 February 2021
Available online 4 March 2021
0266-352X/

Nomenclature

$\acute{\sigma}$	Effective stress
ε	Strain
G, λ	Lame's constants
δ	Kronecker's delta
T	Temperature
$\acute{a}$	Coefficient of thermal volume expansion of the soil particles
u	Soil deflection
σ	Total stress
p_w	Pore water pressure
p_f	Second pore fluid (air or an immiscible fluid) pressure
χ	Bishop's effective stress parameter
F_i	Body force per unit volume of the soil element
e	An indicator for a variation of a parameter
i, j, k	Unit vectors in cartesian coordinate system
ε_v	Volumetric strain
x, y, z	Cartesian coordinates
k_w	Unsaturated permeability of the soil with respect to the water
k_f	Unsaturated permeability of the soil with respect to the second pore fluid phase
ρ	Density
g	Gravitational acceleration
Q	Power output
U, P, Θ, E_v	Transformed form of u, p, T, ε_v after Fourier transformation
I	Imaginary unit
κ	A function of thermal conductivity
D	A complex number
A, B	Constants
Erf	Error function
f	A linear function
R_s	Location of the point heat source in spherical coordinate
R_0	Radius of the spherical heat source
r, z	Location of the object point in cylindrical coordinate
l	Correlations which relate the coefficients to the prime variables
m	Total number of steps in the stepwise method
J	A set of prime variables
K_{unsat}, K_{sat}, K_{dry}	Soil thermal conductivity in unsaturated, saturated, and dry conditions, respectively
ψ	Matric suction
$\beta_e(T)$	Air entry value at the temperature T
k	Soil intrinsic permeability
S_e	Effective degree of saturation
a_w	Coefficient of thermal volume expansion of water
G	Green's function
R	Location of an instantaneous point in spherical coordinate system
t^*	Dimensionless time
μ_w	Water viscosity
μ_f	Second pore fluid viscosity
t	Time
a_u	Coefficient of thermal volume expansion
a_{11}, a_{12}, a_{22}	Apparent compressibility coefficients of the pore fluids
q	Heat generation term
ρc	Volumetric heat capacity
ρ	Mass density
c	Specific heat capacity
P	latent heat of vaporization
θ	Volumetric moisture content
D_θ	Isothermal vapor diffusivity
ϑ	Coefficient of the convection term that accounts for the effects of thermally induced pore water flow on heat transport
v_w	Water velocity
$\mathbf{h}$	Heat flux vector
K	Thermal conductivity
∇	Nabla operator
∇^2	Laplace operator
W	A defined variable
Δ	Dirac delta function
α, β, γ	Real numbers
$\tilde{U}, \tilde{P}, \tilde{\Theta}, \tilde{E}_v$	Transformed form of u, p, T, ε_v after Fourier-Laplace transformation
s	A complex number
$\in, \zeta, \xi, Y, Z, \dot{g}$	Functions of soil properties
Λ	A function of transformed prime variables
R	A spherical coordinate
erfc	Complementary error function
R_{Local}	Distance between the object point and the point heat source
r_s, z_s	Location of the point heat source in cylindrical coordinate
r_0, h	Radius and height of the cylindrical heat source
H	Analytical solution derived in this study
C	A set of coefficients
S	Soil saturation degree
w, a, s	An indicator for water, air, and solid soil, respectively
ψ_0	Initial matric suction
ϖ_T	Surface tension energy at temperature T
k_{rw}	Relative permeability of water
n	Porosity
a_s	Coefficient of thermal volume expansion of the soil
τ	An instantaneous time
n_p	Pore size distribution index
$\varsigma, \eta, \omega, a, b, \phi$	Variables

uncoupled from other governing equations, for the sake of simplicity. In one of the early studies, Booker and Savvidou (Booker and Savvidou, 1985), and Savvidou and Booker (Savvidou and Booker, 1988) developed analytical models, respectively, to predict thermal consolidation around a heat source with constant and decaying heat fluxes in saturated soils. In a separate study, Savvidou and Booker investigated thermal consolidation in soils with anisotropic flow properties (Savvidou and Booker, 1989). Smith and Booker derived Green's function in Laplace and real-time domains for equations governing thermal consolidation in homogeneous soils (Smith and Booker, 1993). Nguyen and Selvadurai (Nguyen and Selvadurai, 1995), and Selvadurai and Nguyen (Selvadurai and Nguyen, 1997) proposed a finite element model to analyze the THM behavior of a rock mass around a waste repository. Bai investigated the response of saturated soils under cyclic thermal loading using the Laplace transformation method (Bai, 2006a). Some studies in the literature analyzed stratified soil response under thermal loads with the aid of the Laplace transformation method (Bai, 2006b), layer element method (Ai and Wang, 2015; Ai and Wang, 2016), propagator matrix method (Yang et al., 2016), and Laplace-Henkel transformation method (Ai et al., 2018).

The above-mentioned analytical models only analyze thermal consolidation in saturated soils and thus, they cannot accurately predict unsaturated thermal consolidation. Nevertheless, in most areas, groundwater is deep and heat sources (e.g. power cables, energy piles/boreholes, and thermally enhanced PVDs) are placed in the vadose zone. Additionally, the mentioned models for saturated thermal consolidation cannot be employed to assess thermal consolidation in soils with two immiscible fluids.

This paper develops a fundamental analytical solution for thermal consolidation around a heat source buried in porous media containing two immiscible pore fluids, or in unsaturated soil comprised of three phases of soil, gas, and liquid (e.g., shallow subsurface soil containing both pore water and pore air). Primary governing equations including equilibrium, pore fluids continuity, and energy balance equations are derived and the analytical solution is provided using Fourier-Laplace transformation based on the solution developed by Booker and Savvidou (Booker and Savvidou, 1985) for saturated thermal consolidation. Then, to consider the variation of the soil thermal, hydraulic, and mechanical properties (e.g., thermal conductivity, degree of saturation, and dynamic viscosity of water) during the thermal consolidation process, a temporal discretized (stepwise linear) method is implemented, so that the coefficients are modified and updated in each time step using the analytical results obtained for the previous time step. The developed solution is compared with the analytical models proposed in the literature for thermal consolidation in saturated soils and the comparison proves the accuracy of the proposed model. Further, the developed analytical model is used to study the difference in THM response (thermal consolidation) of saturated and unsaturated soils.

2. Proposed model

To predict thermal consolidation in three-phase clayey soils, partial differential equations (PDEs) governing coupled thermo-hydro-mechanical behavior of soils including energy, mass, and momentum balance equations are derived. To make the analytical solution possible, it is assumed that the solid soil is incompressible. Local thermal equilibrium is considered between all phases which lead to the same temperature at a single point for all the phases (e.g., soil, water, and air). Additionally, the heat source is assumed to be buried deep enough from the ground surface such that ambient temperature and moisture fluctuations do not affect the results. Please note, previous studies indicated that atmospheric temperature and moisture fluctuations could only change the temperature and moisture content at the very shallow subsurface soils (Olgun, 2013; Tamizdoust and Ghasemi-Fare, 2020b).

In addition to the above-mentioned assumptions, the variations of the soil properties are assumed to be constant within each small time-step. Nevertheless, the changes in these parameters with temperature and pressure increments are considered through the proposed temporal discretized (stepwise linear) method.

The governing equations are derived as follows.

2.1. Incremental constitutive law (the equilibrium of solid skeleton)

The effective stress-strain relationship for an isotropic thermo-elastic medium can be expressed based on Lame's constants as follows:

$$\acute{\sigma}_{ij} = 2G\varepsilon_{ij} + \lambda\varepsilon_{kk}\delta_{ij} - \left(\lambda + \frac{2G}{3}\right)\acute{\alpha}T\delta_{ij} \tag{1}$$

where $\acute{\sigma}_{ij}$ is effective stress, ε_{ij} denotes the strain of the soil skeleton, G, and λ are Lame's constants, δ_{ij} is Kronecker's delta, T is temperature, and $\acute{\alpha}$ is the coefficient of thermal volume expansion of the soil particles. The last term in Eq. (1) indicates the variation of effective stress due to thermal loadings.

The strain of soil skeleton can be defined in terms of displacements as presented below:

$$\varepsilon_{ij} = \frac{1}{2}\left(\frac{\partial u_i}{\partial x_j} + \frac{\partial u_j}{\partial x_i}\right) \quad i,j = 1,2,3 \tag{2}$$

where u_i, u_j are the Cartesian components of deflection, and x_i, x_j are coordinate axes.

Substituting Eq. (2) in Eq. (1) yields predicting effective stress based on displacement vectors.

$$\acute{\sigma}_{ij} = G\left(\frac{\partial u_i}{\partial x_j} + \frac{\partial u_j}{\partial x_i}\right) + \lambda\frac{\partial u_j}{\partial x_j}\delta_{ij} - \left(\lambda + \frac{2G}{3}\right)\acute{\alpha}T\delta_{ij} \tag{3}$$

Bishop's effective stress for three-phase thermo-elastic soil systems can be defined as (Khalili et al., 2004; Vahab and Khalili, 2020):

$$\sigma_{ij} - p_f\delta_{ij} = \acute{\sigma}_{ij} - \chi(p_f - p_w)\delta_{ij} \tag{4}$$

where σ_{ij} and $\acute{\sigma}_{ij}$ are total and effective stresses, respectively, p_w is the pore water pressure, p_f is the second pore fluid (air or an immiscible fluid) pressure, χ is Bishop's effective stress parameter which highly depends on soil saturation degree. $\sigma_{ij} - p_f\delta_{ij}$ denotes net stress. $(p_f - p_w)$ and $\chi(p_f - p_w)$ are known as matric suction and suction stress, respectively (Ghaffaripour et al., 2019; Lu and Likos, 2006).

Eq. (4) can be rearranged as follows:

$$\sigma_{ij} = \acute{\sigma}_{ij} + (1-\chi)p_f\delta_{ij} + \chi p_w\delta_{ij} \tag{5}$$

Combining Eqs. (3) and (5) yields:

$$\sigma_{ij} = G\left(\frac{\partial u_i}{\partial x_j} + \frac{\partial u_j}{\partial x_i}\right) + \lambda\frac{\partial u_j}{\partial x_j}\delta_{ij} + (1-\chi)p_f\delta_{ij} + \chi p_w\delta_{ij} - bT\delta_{ij} \tag{6}$$

where $b = \left(\lambda + \frac{2G}{3}\right)\acute{\alpha}$.

By considering a representative soil volume that is subjected to a total stress σ_{ij}, the equilibrium equation can be expressed as:

$$\frac{\partial\sigma_{ij}}{\partial x_j} + F_i = 0 \quad j = 1,2,3 \tag{7}$$

where F_i is the body force per unit volume of the soil element.

The thermo-elastic deformation in unsaturated soils (or porous media containing two fluid phases) with simultaneous variations of pore fluids pressures and temperature is obtained by combining Eqs. (6) and (7).

$$G\left(\frac{\partial^2 u_i}{\partial x_j\partial x_j} + \frac{\partial^2 u_j}{\partial x_j\partial x_i}\right) + \lambda\frac{\partial^2 u_j}{\partial x_i\partial x_j} + (1-\chi)\frac{\partial p_f}{\partial x_i} + \chi\frac{\partial p_w}{\partial x_i} - b\frac{\partial T}{\partial x_i} + F_i = 0 \tag{8}$$

By considering the variation of the parameters instead of absolute values, and by neglecting the effects of gravity, the equilibrium equation can be simplified as:

$$G\left(\frac{\partial^2 u_i}{\partial x_j\partial x_j} + \frac{\partial^2 u_j}{\partial x_j\partial x_i}\right) + \lambda\frac{\partial^2 u_j}{\partial x_i\partial x_j} + (1-\chi)\frac{\partial p_{ef}}{\partial x_i} + \chi\frac{\partial p_{ew}}{\partial x_i} - b\frac{\partial T_e}{\partial x_i} = 0 \tag{9}$$

where subscript e denotes the variation of a parameter.

Eq. (9) for $i = 1, 2$, and 3 in the Cartesian coordinate system can be demonstrated as follows.

$$\begin{aligned} &G\nabla^2 u_x + (\lambda + G)\frac{\partial\varepsilon_v}{\partial x} + (1-\chi)\frac{\partial p_{ef}}{\partial x} + \chi\frac{\partial p_{ew}}{\partial x} - b\frac{\partial T_e}{\partial x} = 0 \\ &G\nabla^2 u_y + (\lambda + G)\frac{\partial\varepsilon_v}{\partial y} + (1-\chi)\frac{\partial p_{ef}}{\partial y} + \chi\frac{\partial p_{ew}}{\partial y} - b\frac{\partial T_e}{\partial y} = 0 \\ &G\nabla^2 u_z + (\lambda + G)\frac{\partial\varepsilon_v}{\partial z} + (1-\chi)\frac{\partial p_{ef}}{\partial z} + \chi\frac{\partial p_{ew}}{\partial z} - b\frac{\partial T_e}{\partial z} = 0 \end{aligned} \tag{10}$$

where ε_v denotes volumetric strain.

2.2. Pore fluids continuity equations

Excess pore fluids continuity equations based on Darcy's law in general forms can be expressed as Eqs. (11) and (12), respectively (Khalili et al., 2000; Khalili et al., 2008; Shahbodagh-Khan et al., 2015).

$$\frac{k_w}{\mu_w}\left(\nabla^2 p_{ew} + \nabla\rho_w g\right) + \chi\left(\frac{\partial\varepsilon_v}{\partial t} + a_u\frac{\partial T_e}{\partial t}\right) - a_{11}\frac{\partial p_{ew}}{\partial t} - a_{12}\frac{\partial p_{ef}}{\partial t} = 0 \tag{11}$$

$$\frac{k_f}{\mu_f}\left(\nabla^2 p_{ef} + \nabla \rho_f g\right) + (1-\chi)\left(\frac{\partial \varepsilon_v}{\partial t} + a_u \frac{\partial T_e}{\partial t}\right) - a_{12}\frac{\partial p_{ew}}{\partial t} - a_{22}\frac{\partial p_{ef}}{\partial t} = 0 \qquad (12)$$

where k_w and k_f denote the unsaturated permeability of the soil with respect to the water and the second pore fluid phases, respectively. ρ is density, g is gravitational acceleration, μ_w is viscosity of water, μ_f is viscosity of the second pore fluid, t is time, a_u is the coefficient of thermal volume expansion, and a_{11}, a_{12}, and a_{22} are the apparent compressibility coefficients. Subscripts w, and f, respectively represent pore water and the second pore fluid.

The fluids continuity equations presented above for a porous media containing two immiscible incompressible fluids, by neglecting the effects of gravity, can be simplified as:

$$\frac{k_w}{\mu_w}\nabla^2 p_{ew} + \chi\left(\frac{\partial \varepsilon_v}{\partial t} + a_u \frac{\partial T_e}{\partial t}\right) = 0 \qquad (13)$$

$$\frac{k_f}{\mu_f}\nabla^2 p_{ef} + (1-\chi)\left(\frac{\partial \varepsilon_v}{\partial t} + a_u \frac{\partial T_e}{\partial t}\right) = 0 \qquad (14)$$

For the case of unsaturated soil containing water and air (shallow subsurface soil), the air continuity equation is governed by simultaneous Fick's law (diffusion) and Darcy's law (advection). Depending on the soil saturation degree, one of these mechanisms is dominant. When air is in occluded form (higher degrees of saturation) diffusion is dominant. On the contrary, when the air phase is continuous (lower water saturation degrees) advection has a more critical role. Nevertheless, in both cases, the advection-diffusion process leads to the immediate dissipation of pore air pressure due to a high air diffusion coefficient, and higher relative permeability of air compares to water. It has been shown in the literature that excess pore air pressure close to heat sources embedded in the shallow subsurface soil (e.g., geothermal piles, or boreholes, and power cables) dissipates very fast. Consequently, the changes in air pressure are negligible compares to the atmospheric pressure and the thermally induced pore water pressure. Therefore, in several numerical models, pore air pressure has been assumed to be constant and equal to the atmospheric pressure (Novak, 2010; Akrouch et al., 2016; Novak, 2016). Neglecting the changes in air pressure for the case of thermal consolidation in the vadose zone leads to the elimination of the air continuity equation. Thus, Eq. (13) is the sole continuity equation that should be solved for the unsaturated soil containing pore water and pore air. In this case, by considering the equilibrium state, air density can be independently calculated at each step through the ideal gas law. Please note, in this study, equations are solved in a general form. After providing the solution, by considering $p_{ef} = 0$ the solution for the case of unsaturated soil is derived. Please also note, this assumption may not be correct in temperature-controlled unsaturated triaxial tests or experimental-controlled conditions (Khalili et al., 2000).

2.3. Energy conservation equation

Thermal energy balance in unsaturated soil media under hydrostatic condition can be presented as below:

$$-\nabla \mathbf{h} + \rho c \frac{\partial T_e}{\partial t} - q + \vartheta v_w \nabla T_e + \rho P \nabla (D_\theta \nabla \theta) = 0 \qquad (15)$$

where q is the heat generation term, ρc is the volumetric heat capacity of the medium, ρ is mass density, c is specific heat capacity, P is the latent heat of vaporization,θ is the volumetric moisture content, D_θ is the isothermal vapor diffusivity,ϑ is the coefficient of the convection term that accounts for the effects of thermally induced pore water flow on heat transport, v_w is the water velocity, and$\mathbf{h}$ is the heat flux vector and can be calculated based on Fourier's law (Eq. (16)).

$$\mathbf{h} = K \nabla T_e \qquad (16)$$

where K is thermal conductivity.

The last term in the thermal energy balance equation (Eq. (15)) determines the effects of vaporization which depends on many parameters such as soil permeability and saturation degree. In this study, to make the analytical solution possible, the nonlinear evaporation term is neglected. This is an adjustable assumption in modeling fine-grained (e.g. clayey) soils (Hartley and Black, 1981; Rees et al., 2000; Brandl, 2006; Cherati and Ghasemi-Fare, 2019). Therefore, by combining Eqs. (15) and (16), the energy balance equation can be represented as below:

$$\frac{\partial T_e}{\partial t} = \frac{K}{\rho c}\nabla^2 T_e - \frac{\vartheta v_w}{\rho c}\nabla T_e + \frac{q}{\rho c} \qquad (17)$$

To analytically solve the governing equations, a new variable (W) is defined as below.

$$T_e = W \times \exp\left(\frac{\vartheta v_w}{2K}(x+y+z) - \frac{3(\vartheta v_w)^2}{4K}t\right) \qquad (18)$$

The definition of the new parameter (W) helps to combine the effects of both heat conduction and convection. Therefore, the Energy balance equation (Eq. (17)) can be reduced to a new equation in terms of W (Eq. (19)).

$$\frac{\partial W}{\partial t} = \frac{K}{\rho c}\nabla^2 W + \frac{\dot{q}}{\rho c} \qquad (19)$$

where $\dot{q} = q\exp\left(-\frac{\vartheta v_w}{2K}(x+y+z) + \frac{3(\vartheta v_w)^2}{4K}t\right)$.

Therefore, by solving the heat conduction equation (Eq. (19)) and then, changing the main variable using Eq. (18), the solution for coupled heat conduction-convection equation (Eq. (17)) can be obtained. However, since the relative permeability of water in clayey soils is very low, water velocity is negligible (e.g., 10^{-10} m.s^{-1}), claiming that $\exp\left(\frac{\vartheta v_w}{2K}(x+y+z) - \frac{3(\vartheta v_w)^2}{4K}t\right) \approx 1$ (the term inside the parenthesis is almost zero), and thus $T_e \approx W$, and $\dot{q} \approx q$. Therefore, Eq. (19) can be reduced to Eq. (20).

$$\frac{\partial T_e}{\partial t} = \kappa \nabla^2 T_e + \frac{q}{\rho c} \qquad (20)$$

where $\kappa = \frac{K}{\rho c}$.

According to Eq. (20), convection term in the energy balance equation can be neglected in impermeable or very low permeable soils (e.g., clayey soils). The negligible effect of convection term on heat transfer process in soils with relatively low permeability has been acknowledged in several studies (Tamizdoust and Ghasemi-Fare, 2020a; Ghasemi-Fare and Basu, 2019). Tamizdoust and Ghasemi-Fare (2020a) showed that when the permeability is lower than 10^{-13} m^2 (silt and clays) the effect of heat convection in the heat transfer mechanism is negligible and heat conduction can be considered as the sole heat transfer mechanism in the ground. It has also been shown in the literature that the convection term has a considerable effect on heat transfer mechanism in saturated soil only when the permeability is high or the seepage flow passes a threshold (Zhang et al., 2013; Zhang et al., 2014; Wang et al., 2015). Thus, the convection term is neglected in this study, and heat conduction is considered to be the sole mode of heat transport.

2.4. Summary of the governing equations

Equations governing unsaturated thermal consolidation derived in this study are summarized below. Unknown variables of deformations, pore fluids pressures, and temperature can be illustrated as a set of (u, p, T).

$$
\begin{aligned}
&G\nabla^2 u_x + (\lambda+G)\frac{\partial \varepsilon_v}{\partial x} + (1-\chi)\frac{\partial p_{ef}}{\partial x} + \chi\frac{\partial p_{ew}}{\partial x} - b\frac{\partial T_e}{\partial x} = 0\\
&G\nabla^2 u_y + (\lambda+G)\frac{\partial \varepsilon_v}{\partial y} + (1-\chi)\frac{\partial p_{ef}}{\partial y} + \chi\frac{\partial p_{ew}}{\partial y} - b\frac{\partial T_e}{\partial y} = 0\\
&G\nabla^2 u_z + (\lambda+G)\frac{\partial \varepsilon_v}{\partial z} + (1-\chi)\frac{\partial p_{ef}}{\partial z} + \chi\frac{\partial p_{ew}}{\partial z} - b\frac{\partial T_e}{\partial z} = 0\\
&\frac{k_w}{\mu_w}\nabla^2 p_{ew} + \chi\left(\frac{\partial \varepsilon_v}{\partial t} + a_u\frac{\partial T_e}{\partial t}\right) = 0\\
&\frac{k_f}{\mu_f}\nabla^2 p_{ef} + (1-\chi)\left(\frac{\partial \varepsilon_v}{\partial t} + a_u\frac{\partial T_e}{\partial t}\right) = 0\\
&\frac{\partial T_e}{\partial t} = \kappa\nabla^2 T_e + \frac{q}{\rho c}
\end{aligned}
\tag{21}
$$

The physical parameters considered in Eqs. (21) changes with the variation of the prime variables (e.g. temperature and pore pressures) (Khalili and Loret, 2001). However, to make the analytical solution possible, they are assumed to remain constant as a first approximation in this study. Then, the changes in these parameters are considered in time by utilizing a temporal discretized (stepwise linear) approach.

3. Analytical solution for a point heat source

In this section, a solution is developed for a point heat source with the intensity of q located at the origin in an infinite three-phase homogeneous medium.

Dirac delta function is employed according to Eq. (22) to define a point heat source.

$$q = Q\Delta(x)\Delta(y)\Delta(z) \tag{22}$$

where Δ is the Dirac delta function and Q is the power output.

To solve the governing equations analytically, combined Fourier-Laplace transformation is employed. First, Fourier transformation is carried out in x, y, and z directions based on Eq. (23).

$$(U,P,\Theta) = \int_{-\infty}^{\infty}\int_{-\infty}^{\infty}\int_{-\infty}^{\infty} \mathrm{e}^{-\mathrm{i}(\alpha x+\beta y+\gamma z)}(u,p,T)\mathrm{d}x\mathrm{d}y\mathrm{d}z \tag{23}$$

where (U,P,Θ) is the transformed form of (u,p,T) after Fourier transformation, α, β, and γ are real numbers, and i is an imaginary unit.

Laplace transformation is carried out after Fourier transformation according to Eq. (24).

$$\left(\tilde{U},\tilde{P},\tilde{\Theta}\right) = \int_0^{\infty} \mathrm{e}^{-st}(U,P,\Theta)\mathrm{d}t \tag{24}$$

where $\left(\tilde{U},\tilde{P},\tilde{\Theta}\right)$ is the transformed form of (u,p,T) after Fourier-Laplace transformation, and s is a complex number.

The transformed form of the governing equations (Eqs. (21)) can be expressed as Eqs. (25) to (28).

$$
\begin{aligned}
&GD^2\tilde{U}_x = \mathrm{i}\alpha\left[(\lambda+G)\tilde{E}_v + (1-\chi)\tilde{P}_{ea} + \chi\tilde{P}_{ew} - b\tilde{\Theta}\right]\\
&GD^2\tilde{U}_y = \mathrm{i}\beta\left[(\lambda+G)\tilde{E}_v + (1-\chi)\tilde{P}_{ea} + \chi\tilde{P}_{ew} - b\tilde{\Theta}\right]\\
&GD^2\tilde{U}_z = \mathrm{i}\gamma\left[(\lambda+G)\tilde{E}_v + (1-\chi)\tilde{P}_{ea} + \chi\tilde{P}_{ew} - b\tilde{\Theta}\right]
\end{aligned}
\tag{25}
$$

$$\frac{k_w}{\mu_w}\frac{D^2\tilde{P}_{ew}}{s} = \chi\left(\tilde{E}_v + a_u\tilde{\Theta}\right) \tag{26}$$

$$\frac{k_f}{\mu_f}\frac{D^2\tilde{P}_{ef}}{s} = (1-\chi)\left(\tilde{E}_v + a_u\tilde{\Theta}\right) \tag{27}$$

$$\tilde{\Theta}s = -\frac{K}{\rho c}D^2\tilde{\Theta} + \frac{Q}{\rho c} \tag{28}$$

where $D^2 = -(\alpha^2+\beta^2+\gamma^2)$, $E_v = (\mathrm{i}\alpha U_x + \mathrm{i}\beta U_y + \mathrm{i}\gamma U_z)$, and s is the Laplace transform variable.

Eq. (28) can be given as:

$$\tilde{\Theta} = \frac{Q}{K\left(\frac{s\rho c}{K} + D^2\right)} = \frac{Q}{K\left(\frac{s}{\kappa} + D^2\right)} \tag{29}$$

where $\kappa = \frac{K}{\rho c}$.

By merging Eqs. (26) and (27) the transformed excess pore fluid pressure of the second fluid can be expressed as:

$$\tilde{P}_{ef} = \frac{(1-\chi)k_w\mu_f}{\chi\mu_w k_f}\tilde{P}_{ew} \tag{30}$$

If a divergence and then Fourier-Laplace transformation is applied to Eq. (10), the transformed form of volumetric strain E_v can be calculated based on the transformed temperature and excess pore fluids pressures as below.

$$\tilde{E}_v = -\frac{\left((1-\chi)\tilde{P}_{ef} + \chi\tilde{P}_{ew} - b\tilde{\Theta}\right)}{\lambda+2G} \tag{31}$$

Combining Eqs. (30) and (31) results in

$$\tilde{E}_v = -\frac{\epsilon}{\lambda+2G}\tilde{P}_{ew} + \frac{b}{\lambda+2G}\tilde{\Theta} \tag{32}$$

where $\epsilon = \frac{(1-\chi)^2 k_w\mu_f}{\chi\mu_w k_f} + \chi$.

Transformed excess pore water pressure in terms of the transformed excess temperature can be represented by combining Eqs. (26) and (32).

$$\tilde{P}_{ew} = \frac{\xi}{\zeta\frac{D^2}{s} + 1}\tilde{\Theta} \tag{33}$$

where $\zeta = \frac{k_w(\lambda+2G)}{\mu_w\epsilon}$, and $\xi = \frac{a_u(\lambda+2G)-b}{\epsilon}$.

Substituting Eq. (29) in Eq. (33) leads to the transformed excess pore water pressure in terms of the heat intensity.

$$\tilde{P}_{ew} = \frac{\xi}{\left(\zeta\frac{D^2}{s}+1\right)}\frac{Q}{K\left(s/\kappa + D^2\right)} = \frac{\xi Q}{K(1-\zeta/\kappa)}\left[\frac{1}{\left(\frac{s}{\kappa}+D^2\right)} - \frac{1}{\left(\frac{s}{\zeta}+D^2\right)}\right] \tag{34}$$

And transformed second pore fluid pressure variation in terms of the heat intensity can be predicted by combining Eqs. (30) and (34):

$$\tilde{P}_{ef} = \frac{(1-\chi)k_w\mu_f}{\chi\mu_w k_f}\tilde{P}_{ew} = \frac{(1-\chi)k_w\mu_f}{\chi\mu_w k_f}\frac{\xi Q}{K(1-\zeta/\kappa)}\left[\frac{1}{\left(\frac{s}{\kappa}+D^2\right)} - \frac{1}{\left(\frac{s}{\zeta}+D^2\right)}\right] \tag{35}$$

According to Eq. (25), a set of transformed deformations can be expressed as:

$$\left(\tilde{U}_x,\tilde{U}_y,\tilde{U}_z\right) = \Lambda(\mathrm{i}\alpha,\mathrm{i}\beta,\mathrm{i}\gamma) \tag{36}$$

where Λ is $\frac{1}{GD^2}\left[(\lambda+G)\tilde{E}_v + (1-\chi)\tilde{P}_{ea} + \chi\tilde{P}_{ew} - b\tilde{\Theta}\right]$.

By having $\tilde{\Theta}$, $\tilde{E}_v$, $\tilde{P}_{ew}$, and $\tilde{P}_{ef}$ according to Eqs. (29), (32), (34), and (35), it can be indicated that:

$$\Lambda = \frac{Q}{K}a_u\left[\frac{Y}{\left(\frac{s}{\kappa}+D^2\right)D^2} - \frac{Z}{\left(D^2+\frac{s}{\zeta}\right)D^2}\right] \tag{37}$$

where $Y = \frac{1}{\lambda+2G}\left(\frac{a_u(\lambda+2G)-b}{(1-\frac{\zeta}{\kappa})a_u} + \frac{b}{a_u}\right)$, and $Z = \frac{1}{\lambda+2G}\left(\frac{a_u(\lambda+2G)-b}{(1-\frac{\zeta}{\kappa})a_u}\right)$.

Eqs. (29), (34), (35), and (37) are the main transformed equations for the set of main variables (u, p, T) which can be written in the form of $\mathscr{F}(D,s) = \frac{A}{\left(\frac{s}{B}+D^2\right)}$, where A, B are constants. In order to analyze thermal consolidation, it is essential to find the inverse Laplace-Fourier transform of $\mathscr{F}(D,s)$. The inverse transforms in a spherical coordinate system can be calculated much easier by amending a rectangular to a spherical coordinate system:

$$R = \sqrt{(x^2+y^2+z^2)} \tag{38}$$

where R is the location of a point in a spherical coordinate system.

The inverse transform of $\mathscr{F}(D,s)$ in a spherical coordinate can be derived as (See Appendix A):

$$f(R,t) = \frac{A}{4\pi R}\mathrm{erfc}\left(\frac{R}{2\sqrt{Bt}}\right) \tag{39}$$

According to Eq. (39), deformations (u), pore fluids pressures (p), and temperature (T) can be defined as follows:

$$\begin{aligned}
T(R,t) &= \frac{Q}{4\pi KR} f\left(\frac{\kappa t}{R^2}\right)\\
p_{ew}(R,t) &= \frac{\xi}{\left(1-\frac{\zeta}{\kappa}\right)}\frac{Q}{4\pi KR}\left[f\left(\frac{\kappa t}{R^2}\right) - f\left(\frac{\zeta t}{R^2}\right)\right]\\
p_{ef}(R,t) &= \frac{(1-\chi)k_w\mu_f}{\chi\mu_w k_f}\frac{\xi}{\left(1-\frac{\zeta}{\kappa}\right)}\frac{Q}{4\pi KR}\left[f\left(\frac{\kappa t}{R^2}\right) - f\left(\frac{\zeta t}{R^2}\right)\right]\\
\varepsilon_v &= \frac{Q}{(\lambda+2G)4\pi KR}\left[\frac{a_u(\lambda+2G)-b}{\left(1-\frac{\zeta}{\kappa}\right)}\left[f\left(\frac{\kappa t}{R^2}\right) - f\left(\frac{\zeta t}{R^2}\right)\right] + bf\left(\frac{\kappa t}{R^2}\right)\right]\\
u_R(R,t) &= \sqrt{{u_x}^2+{u_y}^2+{u_z}^2} = a_u\frac{Q}{4\pi K}\dot{g}
\end{aligned} \tag{40}$$

where

$$f\left(\frac{\kappa t}{R^2}\right) = \mathrm{erfc}\left(\frac{R}{2\sqrt{\kappa t}}\right)$$

$$g\left(\frac{\kappa t}{R^2}\right) = \frac{\kappa t}{R^2} + \left(\frac{1}{2} - \frac{\kappa t}{R^2}\right)\mathrm{erfc}\left(\frac{R}{2\sqrt{\kappa t}}\right) - \sqrt{\frac{\kappa t}{\pi R^2}}\exp\left(-\frac{R^2}{4\kappa t}\right)$$

$$\dot{g} = Yg\left(\frac{\kappa t}{R^2}\right) - Zg\left(\frac{\zeta t}{R^2}\right)$$

And u_R is the absolute radial deflection in a spherical coordinate system. It comprises three axial components in x, y , and z directions which are obtained easily as $\frac{|x|}{R}a_u\frac{Q}{4\pi K}\dot{g}$, $\frac{|y|}{R}a_u\frac{Q}{4\pi K}\dot{g}$, and $\frac{|z|}{R}a_u\frac{Q}{4\pi K}\dot{g}$, respectively. Moreover, the summation of absolute values results in cumulative (total) deflection.

Eq. (40) is the closed-form solution for thermal consolidation of a porous medium containing two immiscible fluids around a point heat source embedded in an infinite domain and located at the origin.

The axial strains ε_{ij} and stresses σ_{ij} in all directions can be derived by Eqs. (2) and (6) and using the following derivatives:

$$\begin{aligned}
\frac{\partial}{\partial x}\left(\frac{x}{R^2}\mathrm{erfc}(R)\right) &= \frac{\mathrm{erfc}(R)}{R^2} - \frac{2x^2\mathrm{erfc}(R)}{R^4} - \frac{2x^2\exp(-R^2)}{\sqrt{\pi}R^3}\\
\frac{\partial}{\partial y}\left(\frac{x}{R^2}\mathrm{erfc}(R)\right) &= -\frac{2xy\mathrm{erfc}(R)}{R^4} - \frac{2xy\exp(-R^2)}{\sqrt{\pi}R^3}\\
\frac{\partial}{\partial z}\left(\frac{x}{R^2}\mathrm{erfc}(R)\right) &= -\frac{2xz\mathrm{erfc}(R)}{R^4} - \frac{2xz\exp(-R^2)}{\sqrt{\pi}R^3}
\end{aligned} \tag{41}$$

where $R = \sqrt{(x^2+y^2+z^2)}$.

4. Analytical solution for spherical and cylindrical heat sources

In this study, two different heat sources are considered separately with spherical and cylindrical geometry. Then, thermal consolidation in unsaturated soil in the vicinity of each of the heat sources is derived separately based on the developed solution for a point heat. According to Fig. 1 (a), if a point heat source is placed on a line between the object point (the desirable point at which deflections, pressures, and temperature are estimated) and the origin, a general function can be defined based on their distances.

$$f(R_{\mathrm{Local}},t) = f(R-R_s,t) \tag{42}$$

where f is a linear function, $R_{\mathrm{Local}}(=R-R_s)$ is the distance between the object point and the point heat source, R_s is the location of the point heat source, and R is the location of the object point (please see Fig. 1a). When a spherical heat source is buried far enough from the ground surface, the problem can be solved in one-dimensional with respect to radius due to symmetry. Therefore, the solution for the thermal consolidation of unsaturated soils at any point close to a spherical heat source with a radius of R_0 can be derived using Eqs. (40) and (42) and by considering the origin at the center of the sphere (please see Fig. 2a). Please note, in this case, similar to the point heat source, shear stresses and shear strains are equal to zero, due to the symmetry.

$$\begin{aligned}
T(R,t) &= \frac{Q}{4\pi K(R-R_0)} f\left(\frac{\kappa t}{(R-R_0)^2}\right)\\
p_{ew}(R,t) &= \frac{\xi}{\left(1-\frac{\zeta}{\kappa}\right)}\frac{Q}{4\pi K(R-R_0)}\left[f\left(\frac{\kappa t}{(R-R_0)^2}\right) - f\left(\frac{\zeta t}{(R-R_0)^2}\right)\right]\\
p_{ef}(R,t) &= \frac{(1-\chi)k_w\mu_f}{\chi\mu_w k_f}\frac{\xi}{\left(1-\frac{\zeta}{\kappa}\right)}\frac{Q}{4\pi K(R-R_0)}\left[f\left(\frac{\kappa t}{(R-R_0)^2}\right) - f\left(\frac{\zeta t}{(R-R_0)^2}\right)\right]\\
\varepsilon_v &= \frac{Q}{(\lambda+2G)4\pi K(R-R_0)}\left[\frac{a_u(\lambda+2G)-b}{\left(1-\frac{\zeta}{\kappa}\right)}\left[f\left(\frac{\kappa t}{(R-R_0)^2}\right) - f\left(\frac{\zeta t}{(R-R_0)^2}\right)\right] + bf\left(\frac{\kappa t}{(R-R_0)^2}\right)\right]\\
u_R(R,t) &= a_u\frac{Q}{4\pi K}\dot{g}
\end{aligned} \tag{43}$$

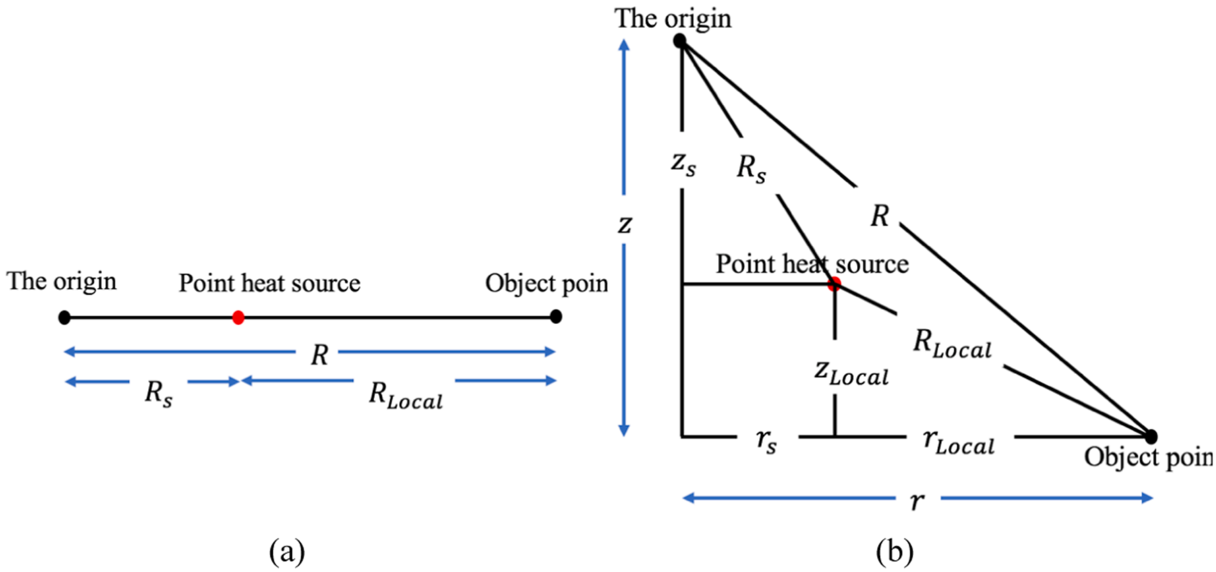

Fig. 1. Schematic of the location of the point heat source and the object point in (a) 1-D condition (Spherical loading), (b) 2-D axisymmetric cylindrical condition.

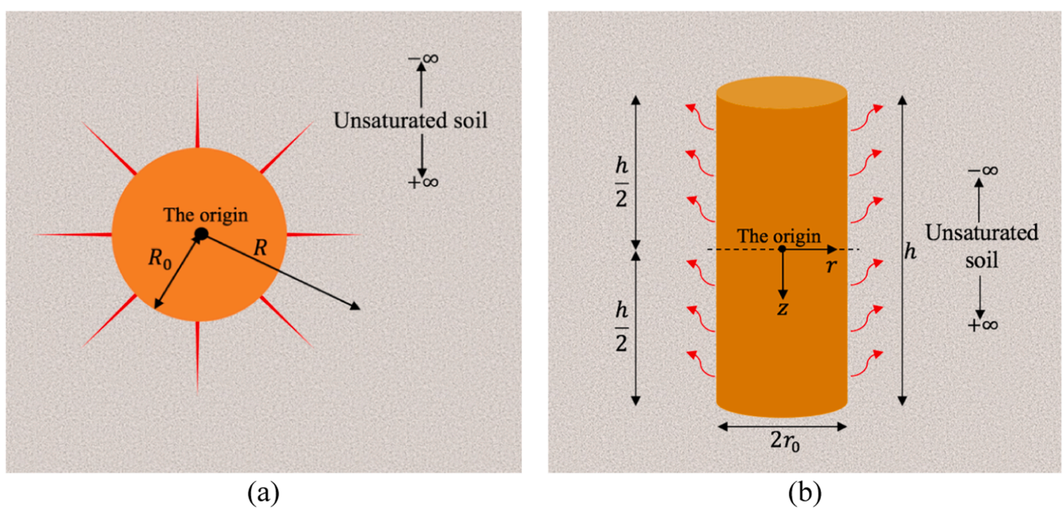

Fig. 2. Schematic configuration of the problem. (a) Spherical heat source (b) Cylindrical heat source.

where $q = \frac{Q\delta(R-R_0)}{4\pi R_0{}^2}$, and $\dot{g} = Yg\left(\frac{\kappa t}{(R-R_0)^2}\right) - Zg\left(\frac{\zeta t}{(R-R_0)^2}\right)$. Note, heat flux ($q$) is defined differently for point, cylindrical, and spherical heat sources.

For the cylindrical heat source, the problem can be solved in a two-dimensional axisymmetric condition (r, z) where, r is the radial coordinate with its origin at the central line passing through the center of the heat source and z is the vertical coordinate which is positive downward (Fig. 2b). Note, to amend a spherical to a cylindrical coordinate, it can be declared that $R = \sqrt{r^2 + z^2}$, where R is a radius in a spherical coordinate.

As mentioned above, in the first step, the presented solution for a point heat source in Eq. (40) should be modified to consider the effect of a point heat source where located in an arbitrary point other than the origin (Fig. 1b). To modify the solution for the cylindrical coordinate system, another relation is defined:

$$f(R_{\mathrm{Local}}, t) = f\left(\sqrt{(r - r_s)^2 + (z - z_s)^2}, t\right) \tag{44}$$

where f is a linear function, R_{Local} is the distance between the object point and the point heat source, (r_s, z_s) is the location of the point heat source, and (r, z) is the location of the object point in a cylindrical coordinate.

Since the derived equations for a point heat source are linear, according to Green's function theory, the superposition technique is valid (Ã–zisik et al., 1993). Thus, the solution for a cylindrical heat source with a radius of r_0 can be derived by integrating the solution of a point heat source on the area of cylinder. By considering the origin at the center of the heat source, the solution in an axisymmetric domain can be derived as (Please see Fig. 2b):

$$
\begin{aligned}
T(r,z,t) &= \int_{-\frac{h}{2}}^{\frac{h}{2}} \frac{Q}{4\pi hK\sqrt{(r-r_0)^2+(z-z_s)^2}} f\left(\frac{\kappa t}{(r-r_0)^2+(z-z_s)^2}\right)\mathrm{d}z_s \\
p_{ew}(r,z,t) &= \int_{-\frac{h}{2}}^{\frac{h}{2}} \frac{\xi}{\left(1-\frac{\zeta}{\kappa}\right)} \frac{Q}{4\pi hK\sqrt{(r-r_0)^2+(z-z_s)^2}}\left[f\left(\frac{\kappa t}{(r-r_0)^2+(z-z_s)^2}\right)-f\left(\frac{\zeta t}{(r-r_0)^2+(z-z_s)^2}\right)\right]\mathrm{d}z_s \\
p_{ef}(r,z,t) &= \int_{-\frac{h}{2}}^{\frac{h}{2}} \frac{(1-\chi)k_w\mu_f}{\chi\mu_w k_f}\frac{\xi}{\left(1-\frac{\zeta}{\kappa}\right)} \frac{Q}{4\pi hK\sqrt{(r-r_0)^2+(z-z_s)^2}}\left[f\left(\frac{\kappa t}{(r-r_0)^2+(z-z_s)^2}\right)-f\left(\frac{\zeta t}{(r-r_0)^2+(z-z_s)^2}\right)\right]\mathrm{d}z_s \\
\varepsilon_v &= \int_{-\frac{h}{2}}^{\frac{h}{2}} \frac{Q}{(\lambda+2G)4\pi K\sqrt{(r-r_0)^2+(z-z_s)^2}}\left[\frac{a_u(\lambda+2G)-b}{\left(1-\frac{\zeta}{\kappa}\right)}\left[f\left(\frac{\kappa t}{(r-r_0)^2+(z-z_s)^2}\right)-f\left(\frac{\zeta t}{(r-r_0)^2+(z-z_s)^2}\right)\right]+bf\left(\frac{\kappa t}{(r-r_0)^2+(z-z_s)^2}\right)\mathrm{d}z_s\right] \\
u_R(r,z,t) &= \int_{-\frac{h}{2}}^{\frac{h}{2}} a_u\frac{Q}{4\pi hK}\dot{g}\mathrm{d}z_s
\end{aligned}
\tag{45}
$$

where $q = \frac{Q\delta(r-r_0)}{2\pi r_0 h}$, $\dot{g} = Yg\left(\frac{\kappa t}{(r-r_0)^2+(z-z_s)^2}\right) - Zg\left(\frac{\zeta t}{(r-r_0)^2+(z-z_s)^2}\right)$, $g\left(\frac{\kappa t}{R^2}\right) = \frac{\kappa t}{R^2} + \left(\frac{1}{2}-\frac{\kappa t}{R^2}\right)\mathrm{erfc}\left(\frac{R}{2\sqrt{\kappa t}}\right) - \sqrt{\frac{\kappa t}{\pi R^2}}\exp\left(-\frac{R^2}{4\kappa t}\right)$, u_R is a deflection vector with two components in r (radial deflection) and z (vertical deflection) directions equal to $\int_{-\frac{h}{2}}^{\frac{h}{2}} \frac{|r-r_0|}{\sqrt{(r-r_0)^2+(z-z_s)^2}} a_u \frac{Q}{4\pi hK}\dot{g}\mathrm{d}z_s$, and $\int_{-\frac{h}{2}}^{\frac{h}{2}} \frac{|z-z_0|}{\sqrt{(r-r_0)^2+(z-z_s)^2}} a_u \frac{Q}{4\pi hK}\dot{g}\mathrm{d}z_s$, respectively. Note, to derive Eq. (45), the origin is considered at the center of the heat source; however, it can be located at any desirable point on the line passing through the center of the source.

The same method can be used to derive a solution for a cubical heat source using Eq. (38).

5. Temporal discretization approach (stepwise linear solution)

In practice, the coefficients in Eqs. (21) (K, χ, k_w, μ_w, …) which represent thermal, hydraulic, and mechanical properties of the soil media vary during the thermal consolidation process with the change of the prime variables (u, p, t). Since analytical solutions can only solve linear equations, the variation of the coefficients cannot be considered in analytical models. This simplifying assumption causes an error that might be noticeable when thermal stresses are enormous. To minimize the error generated by assuming constant coefficients, a temporal discretization approach is adopted in this study, so that the coefficients are updated based on the values of the main variables predicted in the previous time step.

If the set of coefficients (K,χ, k_w, μ_w, …) and the set of prime variables (u, p, t) are represented by C and J, respectively, according to the explained method, for ith time step it can be expressed that:

$$C(i) = l(J(i-1))\&J(i) = H(C(i)) \quad 1 \le i \le m \tag{46}$$

where l denotes the correlations (e.g. a relation between Bishop's effective stress parameter χ, and matric suction) which relate the coefficients to the prime variables, H is the analytical solution derived in the previous section, and m is the total number of time steps.

In the following, to obtain the stepwise solution for unsaturated soils, proposed functions for thermal, hydraulic, and mechanical properties of an unsaturated soil are presented which all are borrowed from the literature. Please note, the same method can be employed for soils with two immiscible fluids.

Thermal conductivity can be predicted based on the soil saturation degree as follows (Johansen, 1977):

$$K_{\mathrm{unsat}} = (\log(S)+1)(K_{\mathrm{sat}}-K_{\mathrm{dry}}) + K_{\mathrm{dry}} \tag{47}$$

where S is the soil saturation degree, and K_{unsat}, K_{sat}, and K_{dry} are soil thermal conductivity in unsaturated, saturated, and dry conditions, respectively.

Volumetric heat capacity of the unsaturated medium can be predicted as below:

$$\rho c = nS(\rho c)_w + n(1-S)(\rho c)_a + (1-n)(\rho c)_s \tag{48}$$

where ρc is volumetric heat capacity, n is porosity, S is saturation degree, and subscripts w, a, and s denote water, gas, and solid soil, respectively.

A relationship between the effective stress parameter and matric suction can be expressed as below (Khalili and Loret, 2001):

$$\chi = \begin{cases} \left[\dfrac{\beta_e(T)}{\psi}\right]^{0.55} & \text{for } \psi \ge \beta_e(T) \\ 1 & \text{for } \psi \le \beta_e(T) \end{cases} \tag{49}$$

where $\psi = \psi_0 - p_{ew}$ is matric suction, ψ_0 is initial matric suction, and $\beta_e(T)$ is the air entry value at the temperature, T, which can be represented in terms of the air entry value at the reference temperature, T_0, as (Khalili and Loret, 2001):

$$\beta_e(T) = \left(\frac{\varpi_T}{\varpi_{T_0}}\beta_e(T_0)\right) \tag{50}$$

where ϖ_T is the surface tension energy at temperature T which is approximated as (Hilgardia, 1943):

$$\varpi = 0.1171 - 0.0001516T \tag{51}$$

The following relationship to predict water permeability is proposed by Brooks and Corey (Brooks and Corey, 1966).

$$k_w = k \times k_{rw} = k \times S_e^{\frac{2+3n_p}{n_p}} \tag{52}$$

where k is the soil intrinsic permeability, k_{rw} is the relative permeability of water, S_e is an effective degree of saturation and is considered equal to χ in this study, and n_p is the pore size distribution index.

The dynamic viscosity of water can be represented as:

$$\mu_w = 2.5 \times 10^{-5} \times 10^{248/(T+133)} \tag{53}$$

Thermal volume expansion of the unsaturated medium can be estimated as below:

$$a_u = nSa_w + (1-n)a_s \tag{54}$$

where a is thermal expansion coefficient, n is porosity, S is saturation degree, and subscripts w and s denote water, and solid soil, respectively.

The above-mentioned relations are used in the temporal discretized (stepwise linear) model to derive an accurate solution for unsaturated thermal consolidation.

6. Validation

The validation is carried out in three steps separately for the governing equations, the proposed solution, and the analytical results.

Step 1: For the first step, the derived equations in this study for the special case of saturated soil are compared with the equations proposed in the literature for saturated thermal consolidation. The derived equations in this study for the saturated state ($\chi = 1$) can be represented as below:

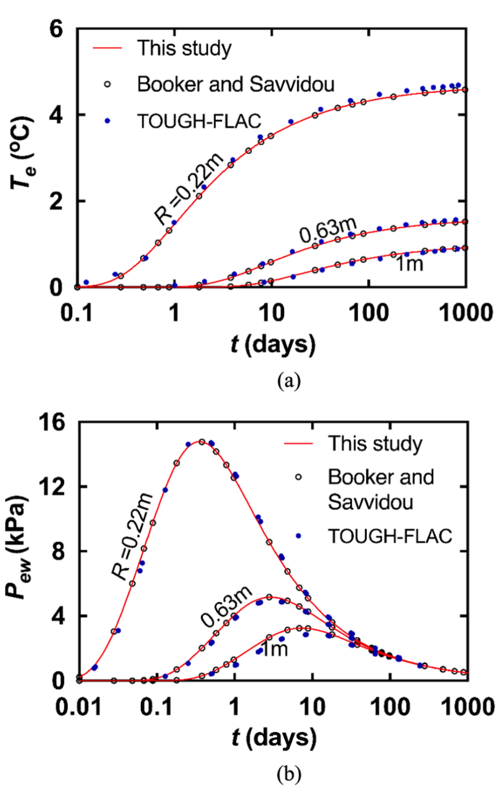

Fig. 3. Comparison of thermal consolidation around a point heat source in saturated condition ($\chi = 1$) for (a) excess temperature and (b) excess pore water pressure obtained in this study by the results presented by Booker and Savvidou (1985) and Blanco-Martín et al. (2017).

$$\begin{aligned}
&G\nabla^2 u_x + (\lambda + G)\frac{\partial \varepsilon_v}{\partial x} + \frac{\partial p_{ew}}{\partial x} - b\frac{\partial T}{\partial x} = 0\\
&G\nabla^2 u_y + (\lambda + G)\frac{\partial \varepsilon_v}{\partial y} + \frac{\partial p_{ew}}{\partial y} - b\frac{\partial T}{\partial y} = 0\\
&G\nabla^2 u_z + (\lambda + G)\frac{\partial \varepsilon_v}{\partial z} + \frac{\partial p_{ew}}{\partial z} - b\frac{\partial T}{\partial z} = 0\\
&\frac{k_w}{\mu_w}\nabla^2 p_{ew} + \frac{\partial \varepsilon_v}{\partial t} + a_u\frac{\partial T}{\partial t} = 0\\
&\frac{\partial T}{\partial t} = \kappa \nabla^2 T + \frac{q}{\rho c}
\end{aligned} \tag{55}$$

Eqs. (55) are consistent with the equations presented by Booker and Savvidou for thermal consolidation in saturated soils (Booker and Savvidou, 1985). Note, there is no second pore fluid continuity equation when $\chi = 1$ (saturated state).

The developed equations in this study for the unsaturated condition are also consistent with the equations proposed in the literature for THM analysis of unsaturated soils (Khalili et al., 2000; Khalili et al., 2008; Shahbodagh-Khan et al., 2015).

Step 2: To validate the solution approach for a point heat source, the accuracy of the solution proposed in Eq. (40) needs to be evaluated. However, since the same analytical approach (Eq. (39)) has been employed to solve the PDEs for all four parameters (excess pore fluids pressures, displacement, and temperature), validating one of them (e.g., temperature variations) confirms the accuracy of the solution approach. To validate the provided solution for the heat conduction equation, Green's function method is employed. Green's function estimates the effects of a point heat source with unit intensity at time t, located at $\acute{R}$ activated at an instantaneous time τ on a point in the domain located at R (Ã–zisik et al., 1993; Cole et al., 2010). Green's function for heat conduction around a point heat source embedded in the ground in a spherical coordinate system can be expressed as (Ã–zisik et al., 1993; Cole et al., 2010):

$$G(R,t|\acute{R},\tau) = \frac{1}{[4\pi\kappa(t-\tau)]^{3/2}}\exp\left[-\frac{(R-\acute{R})^2}{4\kappa(t-\tau)}\right] \tag{56}$$

To evaluate the effects of a heat source on the adjacent soil from 0 to t (by considering $\tau = 0$ and $\acute{R} = 0$) Green's function should be integrated with respect to time from 0 to t.

$$T = \int_0^t \frac{1}{[4\pi\kappa(t-\tau)]^{3/2}}\exp\left[-\frac{R^2}{4\kappa(t-\tau)}\right]d\tau \tag{57}$$

The solution for the above integration (Eq. (57)) using Green's function method (Please see Appendix B), matches with the solution provided in this study in Eq. (40).

Step 3: In the last step, temperature increment and excess pore water pressure around a point heat source predicted in this study are compared

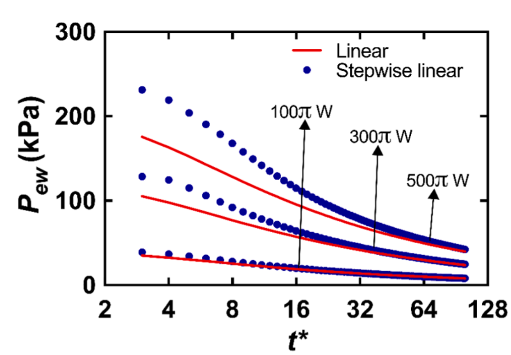

Fig. 4. Comparison of excess pore water pressure derived from linear and stepwise linear solutions for $Q = 100\pi$W, 300πW, and 500πW at $R = 1$m around a point heat source.

with the solutions proposed by Booker and Savvidou (1985) and Blanco-Martín et al. (2017) for a saturated soil (specific condition when $\chi = 1$). In the latter study, the authors employed TOUGH-FLAC simulator to predict temperature and pore water pressure at distances of $R = 0.22$, $0.63, \mathrm{and} 1\mathrm{m}$ from a point heat source while considering, $\chi = 1$, $E = 0.65\times 10^9\mathrm{Pa}$, $\xi = 5.5\times 10^3\mathrm{Pa.K^{-1}}$, $\zeta = 1.63\times 10^{-5}\mathrm{m^2s^{-1}}$, $K = 1.2\mathrm{W.m^{-1}.K^{-1}}$, $\kappa = 1.09\times 10^{-6}\mathrm{m^2s^{-1}}$, $Q = 15.6\mathrm{W}$, and $\rho c = 4.4\times 10^6\mathrm{Jm^{-3}K^{-1}}$.

Fig. 3 (a) and (b) compare the temperature increment and excess pore water pressure around a point heat source estimated using the analytical solution provided in this study with the analytical solution available in the literature for a saturated soil (Booker and Savvidou, 1985; Blanco-Martín et al., 2017). As it can be seen in Fig. 3, the proposed analytical solution for $\chi = 1$ is consistent with the available models.

7. Results and discussion

In order to present the results, first, linear and stepwise linear solutions proposed in this study are compared to show the errors caused by considering constant soil properties during unsaturated thermal consolidation around a point heat source. Then, the effects of soil saturation degree on the THM behavior of unsaturated soil are assessed by comparing thermal consolidation of saturated and unsaturated soils around a point heat source. Finally, unsaturated thermal consolidation around spherical and cylindrical heat sources are analyzed separately. A representative spherical heat source with $R_0 = 1\mathrm{m}$ and a cylindrical heat source with $r_0 = 1\mathrm{m}$ and $h = 10\mathrm{m}$ stretched from $z = -5\mathrm{m}$ to $z = 5\mathrm{m}$ buried in an unsaturated soil are considered separately. The variation of pore air pressure during thermal loading in the shallow subsurface is neglected. The initial parameters required for numerical study are considered as follows: $\frac{k_w}{\mu_w} = 0.2\times 10^{-12}\mathrm{m^{-3}.s.kg^{-1}}$, $\frac{k_f}{\mu_f} = 0.2\times 10^{-8}\mathrm{m^{-3}.s.kg^{-1}}$, $\chi = 0.8$, $\lambda + 2G = 0.5\times 10^9\mathrm{Pa}$, $a_u = 0.2\times 10^{-4}\mathrm{K^{-1}}$, $b = 0.25\times 10^4\mathrm{Pa.K^{-1}}$, $K = 1\mathrm{W.m^{-1}.K^{-1}}$, $\kappa = 7\times 10^{-5}\mathrm{m^2s^{-1}}$ and $Q = 100\pi\mathrm{W}$, $n = 1.5$. Dimensionless time in spherical and cylindrical coordinates are defined as $t^* = \frac{4\kappa t}{{R_0}^2}$ and $t^* = \frac{4\kappa t}{{r_0}^2}$, respectively. Please note, compressive stresses and strains are considered positive in this study.

7.1. Comparison of linear and stepwise linear solutions

To investigate the error caused by neglecting the variation of coefficients, the linear and stepwise linear solutions for pore water pressure around a point heat source are compared for three different values of heat intensity ($Q = 100\pi\mathrm{W}, 300\pi\mathrm{W}$, and $500\pi\mathrm{W}$). Other parameters are kept constant. Fig. 4 compares the values of pore water pressure obtained by linear and stepwise linear solutions. When $Q = 100\pi\mathrm{W}$ the error is negligible since lower heat intensity (thermal loading) has a limited effect on thermal, hydraulic, and mechanical properties of the soil media. Thus, for lower amounts of the heat flux (lower than $100\pi\mathrm{W}$), the closed form solution proposed in this study accurately predicts the unsaturated thermal consolidation. However, for $Q = 500\pi\mathrm{W}$, the changes in temperature and pore water pressure are considerable. Thus, the variation of the coefficients is tangible and consequently, the error induced by employing the linear solution cannot be ignored when temperature changes are significant. Consequently, the stepwise method should be employed.

7.2. Effects of saturation degree

To analyze the performance of the proposed analytical model for the unsaturated soil state, temperature variation, excess pore water pressure, and soil deflection in saturated soil ($\chi = 1$) are compared with the analytical model considering different values of effective degree of saturation ($\chi = 1, 0.8, \mathrm{and} 0.6$). Soil parameters in saturated state ($\chi = 1$) are considered same as previous sections. However, to accurately model the unsaturated condition, all the soil parameters at the 80% and 60% saturation degrees ($\chi = 0.8 \mathrm{and} 0.6$) are updated by using Eqs. (47)–(54). Fig. 5 compares thermal consolidation for different values of χ. As it can

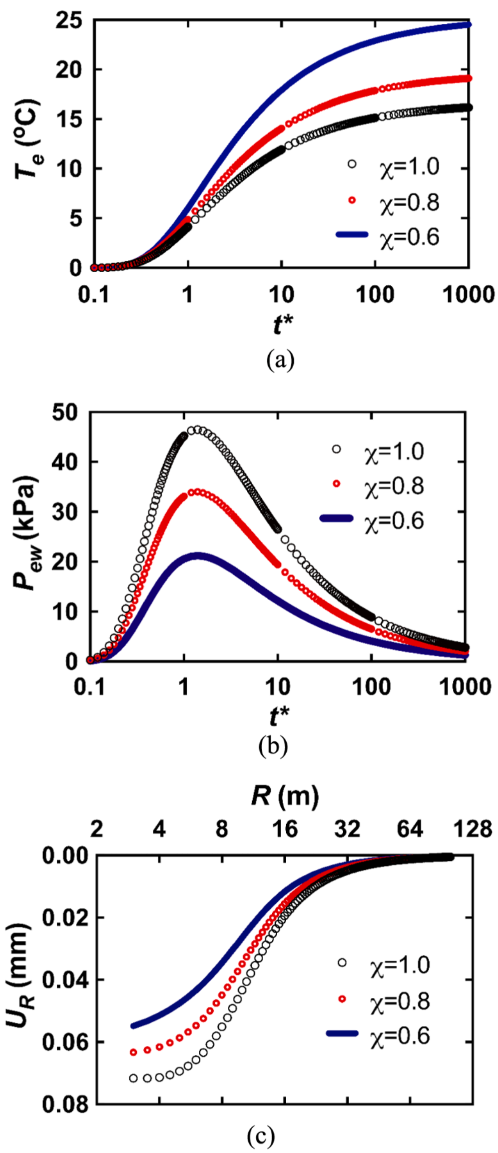

Fig. 5. Variation of (a) temperature at $R = 1\mathrm{m}$, (b) pore water pressure at $R = 1\mathrm{m}$, and (c) deflection at $t^* = 10$ for different values of Bishop's effective stress parameter (effective saturation degree).

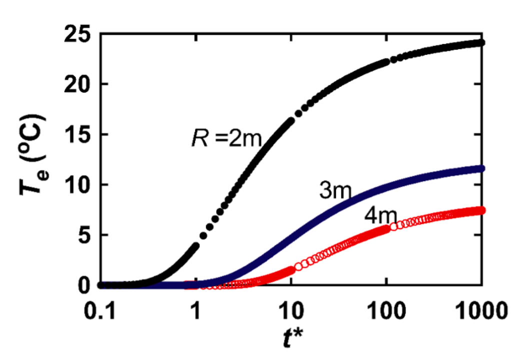

Fig. 6. Temperature variations at different locations close to the spherical heat source.

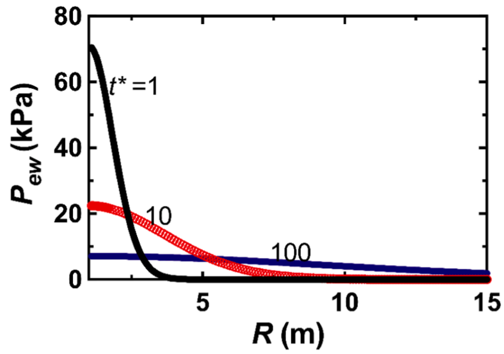

Fig. 7. Variation of excess pore water pressure in radius from the core of the spherical heat source.

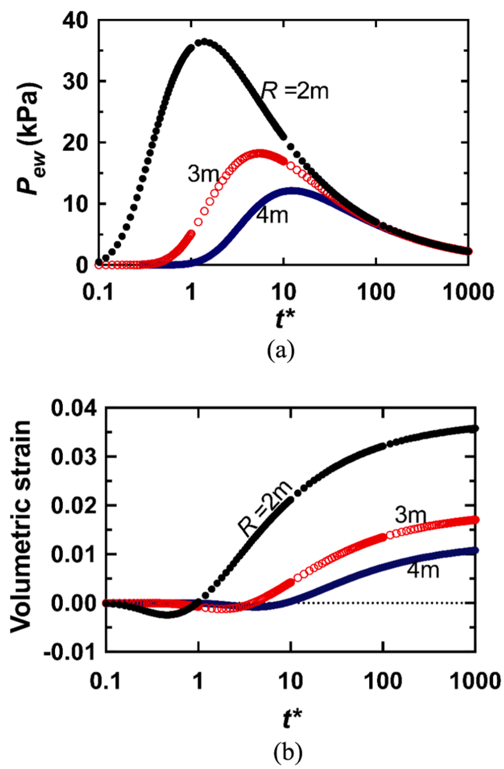

Fig. 8. Variations of (a) excess pore water pressure, and (b) volumetric strain at different points close to the spherical heat source.

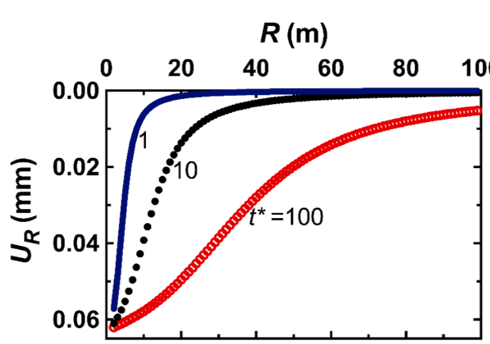

Fig. 9. Thermal absolute displacement in radius at different time steps for the spherical heat source.

be seen in the figure, soil temperature increment is higher when the χ is lower. This happens because of reduction in thermal conductivity for lower effective degree of saturation. This is compatible with the results presented in the literature which compared the heat transfer in saturated and dry soils (Ghasemi-Fare and Basu, 2018). However, in saturated soil, due to the higher amount of water, the thermal volume change (thermal expansion) of the pore water in the soil medium is larger, and therefore, as it is expected, the excess pore water pressure is higher for the saturated condition. Furthermore, matric suction in unsaturated soil increases the soil strength and consequently, under the same thermal stress, unsaturated soil undergoes a lower deflection in comparison with saturated soil. Fig. 5 (c) indicates soil deflection in radius at $t^* = 10$ for different values of χ. As it can be seen, the analytical model demonstrates higher deflection when χ increases. Hence, these comparisons prove the applicability of this model for predicting thermal consolidation in both saturated and unsaturated conditions.

7.3. Unsaturated thermal consolidation around a spherical heat source

In this section, unsaturated thermal consolidation around a spherical heat source with $R_0 = 1\mathrm{m}$ is investigated by using the stepwise linear method. Figs. 6–9 present thermal consolidation in the unsaturated soil around the spherical heat source. Fig. 6 shows temperature variations over time at different points. Temperature undergoes a tremendous surge very close to the heat source ($R = 2$) and reaches an asymptotic value at farther points. As can be seen, the intensity of temperature growth alleviates over time and thus, it is expected that pore pressure generation rate reduces gradually.

Fig. 7 determines the variation of excess pore water pressure from the core of the spherical heat source. The figure illustrates a drastic dissipation of excess pore water pressure for zones close to the heat source ($R < 2$) in a short time (e.g., from $t^* = 1$ to $t^* = 10$) while, in farther points, excess pore water pressure generation is still superior.

Fig. 8 (a) and (b), respectively, present the changes in excess pore water pressure and the volumetric strain (thermal volume change) evolution over time at three different radial distances from the core of the heat source. During the early stage of thermal loading, pore fluid and solid soils expand. However, due to the difference in thermal expansion coefficients of the pore volume and the pore fluid, excess pore fluid pressure is generated. As it can be seen in Fig. 8 (a), excess pore water pressure generation is not a sudden phenomenon and it continues with a decaying intensity due to the transient nature of the thermal loading. It also demonstrates that excess pore water pressure generation starts earlier at the points closer to the heat source. Then, at a later time, by alleviating the temperature increment, the generation rate wanes and the dissipation will be dominant. Therefore, excess pore water pressure, which depends on both generation and dissipation rates, decreases and thermal volume reduction (thermal consolidation) happens due to the outflow of the fluid. Results presented in Fig. 8 (b) shows initial thermal

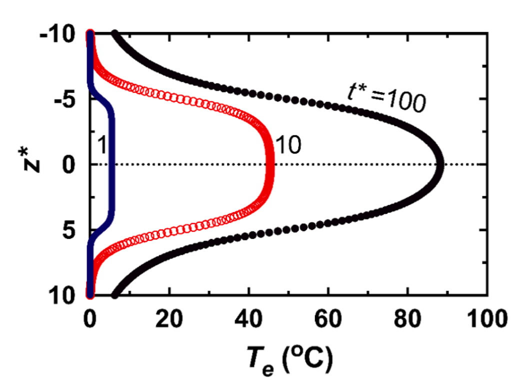

Fig. 10. Temperature increments along the depth of the cylindrical heat source at $r = 2$.

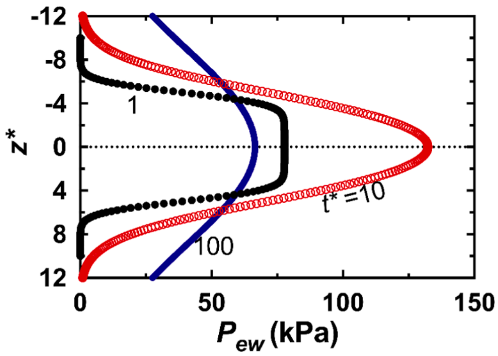

Fig 11. Variations of excess pore water pressure along the depth for the cylindrical heat source at $r = 2$.

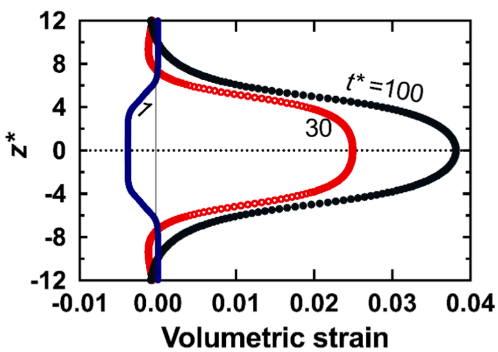

Fig. 12. Volumetric strain along depth for the cylindrical heat source at $r = 2$.

volume expansion in the medium before starting the dissipation of pore fluid pressure. Please note, negative volumetric strain denotes thermal expansion. Thermal expansion and excess pore water pressure generation happen immediately close to the heat source. Then, excess pore water pressure starts to dissipate in zones close to the heat source while thermal expansion and excess pore water pressure generation occur at farther zones. Fig. 8 (a) and (b) demonstrate initial expansion and higher initial excess pore water generation rate which follow by higher dissipation rate and volume reduction. However, the time corresponding to the domination of volume reduction (the peak points in the figures) depends on the distance of the object point from the heat source. Note, the dissipation rate depends on pore size distribution in the medium and thus, the thermal consolidation process in unsaturated soil varies for clays with different permeability values.

In the next step, thermal radial displacement close to the spherical heat source is analyzed. Fig. 9 confirms that thermal deflection reaches its maximum value very close to the heat source in a short period. It also depicts the progress in the thermal consolidation influence zone (where the deflection is bigger than zero) which increases from $R = 30$ at $t^* = 1$ to $R = 80$ at $t^* = 10$.

7.4. Unsaturated thermal consolidation around a cylindrical heat source

A heat source with $r_0 = 1\text{m}$ and $h = 10\text{m}$ (from $z = -5\text{m}$ to $z = 5\text{m}$) is considered to present the result for the thermal consolidation in unsaturated soil around a cylindrical heat source. Fig. 10 demonstrates the temperature increment at $r = 2$ along the depth. The result indicates an almost identical temperature increase along the depth at $r = 2$ in relatively shorter times ($t^* = 1$) while the temperature increment rate is higher at the center axis due to the accumulation of heat.

Fig. 11 demonstrates the variation of pore water pressure along the depth of the heat source at $r = 2$. It can be seen that at the early stage of thermal loading (at $t^* = 1$) identical excess pore water pressure generated between $z = -4$ to 4. Comparing temperature increment and pore water pressure at the $z = 0$ in Figs. 10 and 11 at $t^* = 10$ and 100 indicate that excess pore fluid pressure reaches the maximum value while the temperature is still increasing. This confirms that the dissipation of the pore water pressure can be dominant even during the thermal loading. That is to say, there are thermal expansion and pore water pressure generation from $t^* = 10$ to $t^* = 100$; however, the rate of consolidation and pore pressure dissipation is dominant. Fig. 11 also shows while dissipation of pore water pressure close to the heat source (from $z = -6$ to 6) is dominant from $t^* = 10$ and $t^* = 100$, during the same time, pore fluid pressure generation is dominant at the farther zones ($z > 6orz < -6$).

Fig. 12 presents volumetric strain evolution over time along the depth of the heat source. According to Fig. 12, initially, at $t^* = 1$ soil close to the heat source tends to expand, but gradually with the dissipation of the pore fluid pressure, thermal volume reduction is visible. It is also interesting to note that, while thermal consolidation happens in the zones closer to the heat source, thermal expansion is still the primary mechanism that determines the soil behavior in farther zones.

8. Conclusion

Thermal consolidation in porous media is a challenging problem in various engineering fields. The available analytical models for soil thermal consolidation are derived for the fully saturated condition. While in several cases heat sources are buried in the vadose zone or a porous medium with two immiscible pore fluids. Thus, thermal consolidation needs to be analyzed in a three-phase soil system. In this paper, a fundamental analytical solution for thermal consolidation in three-phase fine-grained soils (e.g., unsaturated thermal consolidation in clayey soils) in the vicinity of an embedded heat source is developed based on the effective stress concept. The developed model considers the variation of pore water pressure, and displacements induced by transient heat transfer in a thermo-elastic soil medium around a heat source. PDEs governing thermo-hydro-mechanical behavior of three-phase soils are developed and the solution is derived by employing Fourier-Laplace transformation. The inverse transformation is carried out fully analytically and thus, a closed-form solution is developed. Then, to consider the variation of the soil properties (coefficients in the governing equations) during the thermal consolidation process, a temporal discretization method is implemented. The analytical model is validated through a three-step validation process including validating the developed equations, the derived solution, and the results. The variation of excess pore fluid pressures, volumetric strain, and soil displacement are studied around both spherical and cylindrical heat sources. The analytical results demonstrate while temperature increases, the excess pore fluid pressures may drop. Moreover, while unsaturated thermal consolidation occurs in points closer to the heat source, thermal expansion, and excess pore fluid generation can be still dominant in farther zones.

CRediT authorship contribution statement

Davood Yazdani Cherati: Resources, Formal analysis, Investigation, Methodology, Data curation, Writing - original draft, Writing - review & editing. **Omid Ghasemi-Fare:** Project administration, Conceptualization, Methodology, Funding acquisition, Supervision, Data curation, Writing - original draft, Writing - review & editing.

Declaration of Competing Interest

The authors declare that they have no known competing financial interests or personal relationships that could have appeared to influence the work reported in this paper.

Acknowledgments

The second author would also like to gratefully acknowledge the financial support from the National Science Foundation under Grant No. CMMI-1804822.

Appendix A

The inverse Fourier transformation of $\frac{A}{\left(\frac{s}{B}+D^2\right)}$ in a spherical coordinate system can be expressed as:

$$\frac{A}{(2\pi)^3}\int_0^{\infty}\int_0^{\pi}\int_0^{2\pi}\frac{\exp(\mathrm{i}RD\sin(\eta))}{\left(D^2+\frac{s}{B}\right)}\cos(\eta)D^2\mathrm{d}\varsigma\mathrm{d}\eta\mathrm{d}D \tag{A.1}$$

Integrating with respect to ς yields:

$$\frac{A}{(2\pi)^2}\int_0^{\infty}\int_0^{\pi}\frac{\exp(\mathrm{i}RD\sin(\eta))}{\left(D^2+\frac{s}{B}\right)}\cos(\eta)D^2\mathrm{d}\eta\mathrm{d}D \tag{A.2}$$

Then, by integrating with respect to η Eq. (A.2) can be simplified as below:

$$\frac{A}{(2\pi)^2}\int_0^{\infty}\left[\frac{\exp(\mathrm{i}RD\sin(\eta))}{\mathrm{i}RD}\right]\begin{matrix}\pi\\0\end{matrix}\frac{D^2}{\left(D^2+\frac{s}{B}\right)}\mathrm{d}D \tag{A.3}$$

Due to the nature of the problem and since parameters in this study only adapt real numbers, the real part of Eq. (A.3) should be considered. Using Euler's formula $\exp(\mathrm{i}x)=\cos x+\mathrm{i}\sin x$, and considering $\frac{1}{\mathrm{i}}=-\mathrm{i}$, the real part of Eq. (A.3) can be written as:

$$\frac{A}{(2\pi)^2R}\int_0^{\infty}2\sin(RD)\frac{D}{\left(D^2+\frac{s}{B}\right)}\mathrm{d}D \tag{A.4}$$

Inverse Fourier transform of $\frac{A}{\left(\frac{s}{B}+D^2\right)}$ is derived by solving Eq. (A.4), as follows:

$$F(R,s)=\frac{A}{4\pi R}\exp\left(-\sqrt{\frac{s}{B}}R\right) \tag{A.5}$$

Calculating the inverse Laplace transform of Eq. (A.5) yields:

$$f(R,t)=\frac{A}{4\pi R}\mathrm{erfc}\left(\frac{R}{2\sqrt{Bt}}\right) \tag{A.6}$$

Appendix B

By considering $t-\tau=\omega$ Eq. (57) could be restated as below:

$$T=-\frac{1}{[4\pi\kappa]^{3/2}}\int_0^t\frac{1}{\omega^{3/2}}\exp\left[-\frac{R^2}{4\kappa\omega}\right]\mathrm{d}\omega \tag{B.1}$$

where $\mathrm{d}\omega=-\mathrm{d}\tau$.

In order to solve Eq. (B.1), it is needed to come up with a solution for the integration below:

$$\int\frac{1}{\omega^{3/2}}\exp\left[-\frac{a^2}{\omega}\right]\mathrm{d}\omega \tag{B.2}$$

where $=\frac{R}{2\sqrt{\kappa}}$.

To solve Eq. (B.2), a new variable is defined as $\omega^{-\frac{1}{2}}=\phi$. Thus, Eq. (B.2) could be rearranged with respect to the new variable as:

$$\int\frac{1}{\omega^{3/2}}\exp\left[-\frac{a^2}{\omega}\right]\mathrm{d}\omega=-2\int\exp\left[-a^2\phi^2\right]\mathrm{d}\phi \tag{B.3}$$

The error function is defined as: $\int\exp(-b^2x^2)\mathrm{d}x=\frac{\sqrt{\pi}}{2b}\mathrm{erf}(bx)$.

Eq. (B.3) can be rearranged using the Error function as below

$$\int\frac{1}{\omega^{3/2}}\exp\left[-\frac{a^2}{\omega}\right]\mathrm{d}\omega=-2\int\exp\left[-a^2\phi^2\right]\mathrm{d}\phi=-\frac{\sqrt{\pi}}{a}\mathrm{erf}(a\phi) \tag{B.4}$$

By using Eq. (B.4), soil temperature response (Eq. (B.1)) can be expressed as:

$$T=-\frac{1}{4\pi\kappa R}\left[\mathrm{erf}\left(\frac{R}{\sqrt{4\kappa\omega}}\right)\right]_0^t=-\frac{1}{4\pi\kappa R}\left[\mathrm{erf}\left(\frac{R}{\sqrt{4\kappa t}}\right)-1\right] \tag{B.5}$$

Complementary error function is defined as $\mathrm{erfc}(x) = 1 - \mathrm{erf}(x)$. Therefore, Eq. (B.5) can be expressed as below:

$$T = \frac{1}{4\pi\kappa R}\left[\mathrm{erfc}\left(\frac{R}{\sqrt{4\kappa t}}\right)\right] \tag{B.6}$$

Eq. (B.6) predicts soil temperature variation induced by a point heat source with unit intensity. Thus, for a point heat source with the intensity of $\frac{Q}{\rho c}$, temperature evolution could be calculated as below:

$$T = \frac{\frac{Q}{\rho c}}{4\pi\kappa R}\left[\mathrm{erfc}\left(\frac{R}{\sqrt{4\kappa t}}\right)\right] = \frac{Q}{4\pi K R}\left[\mathrm{erfc}\left(\frac{R}{\sqrt{4\kappa t}}\right)\right] \tag{B.7}$$

where $\kappa = \frac{K}{\rho c}$.

References

Abdel-Hadi, O.N., Mitchell, J.K., 1981. Coupled heat and water flows around buried cables. J. Geotech. Geoenviron. Eng. 107.

Abousleiman, Y., Ekbote, S., 2005. Solutions for the inclined borehole in a porothermoelastic transversely isotropic medium. J. Appl. Mech. 72, 102–114.

Abuel-Naga, H.M., Bergado, D.T., Ramana, G.V., Grino, L., Rujivipat, P., Thet, Y., 2006. Experimental evaluation of engineering behavior of soft Bangkok clay under elevated temperature. J. Geotech. Geoenviron. Eng. 132, 902–910.

Ai, Z.Y., Wang, L.J., 2016. Three-dimensional thermo-hydro-mechanical responses of stratified saturated porothermoelastic material. Appl. Math. Model. 40, 8912–8933.

Ai, Z.Y., Wang, L.J., 2015. Axisymmetric thermal consolidation of multilayered porous thermoelastic media due to a heat source. Int. J. Numer. Anal. Meth. Geomech. 39, 1912–1931. https://doi.org/10.1002/nag.2381.

Ai, Z.Y., Ye, Z., Zhao, Z., Wu, Q.L., Wang, L.J., 2018. Time-dependent behavior of axisymmetric thermal consolidation for multilayered transversely isotropic poroelastic material. Appl. Math. Model. 61, 216–236.

Akrouch, G.A., Sánchez, M., Briaud, J.-L., 2016. An experimental, analytical and numerical study on the thermal efficiency of energy piles in unsaturated soils. Comput. Geotech. 71, 207–220.

Asefzadeh, A., 2019. Thermo-mechanical performance evaluation of pavement materials in cold regions.

Ã–zisik, M.N., Özısık, M.N., Özışık, M.N., 1993. Heat Conduction. John Wiley & Sons.

Bai, B., 2006a. Fluctuation responses of saturated porous media subjected to cyclic thermal loading. Comput. Geotech. 33, 396–403. https://doi.org/10.1016/j.compgeo.2006.08.005.

Bai, B., 2006b. Thermal consolidation of layered porous half-space to variable thermal loading. Appl. Math. Mech. 27, 1531–1539. https://doi.org/10.1007/s10483-006-1111-1.

Biot, M.A., 1941. General theory of three-dimensional consolidation. J. Appl. Phys. 12, 155–164.

Blanco-Martín, L., Rutqvist, J., Birkholzer, J.T., 2017. Extension of TOUGH-FLAC to the finite strain framework. Comput. Geosci. 108, 64–71.

Booker, J.R., Savvidou, C., 1985. Consolidation around a point heat source. Int. J. Numer. Anal. Meth. Geomech. 9, 173–184.

Brandl, H., 2006. Energy foundations and other thermo-active ground structures. Géotechnique 56, 81–122.

Brooks, R.H., Corey, A.T., 1966. Properties of porous media affecting fluid flow. J. Irrig. Drainage Div. 92, 61–90.

Cherati, D.Y., Ghasemi-Fare, O., 2019. Analyzing transient heat and moisture transport surrounding a heat source in unsaturated porous media using the Green's function. Geothermics 81, 224–234.

Cherati, D.Y., Ghasemi-Fare, O., Senejani, H.H., 2020. Effects of different parameters on transient heat transfer surrounding energy piles in unsaturated soils. E3S Web Conf. 205, 05015. https://doi.org/10.1051/e3sconf/202020505015.

Coccia, C.J.R., McCartney, J.S., 2016. Thermal volume change of poorly draining soils I: critical assessment of volume change mechanisms. Comput. Geotech. 80, 26–40.

Cole, K., Beck, J., Haji-Sheikh, A., Litkouhi, B., 2010. Heat Conduction using Greens Functions. Taylor & Francis.

de Lieto Vollaro, R., Fontana, L., Vallati, A., 2011. Thermal analysis of underground electrical power cables buried in non-homogeneous soils. Appl. Therm. Eng. 31, 772–778.

Falcone, G., Liu, X., Okech, R.R., Seyidov, F., Teodoriu, C., 2018. Assessment of deep geothermal energy exploitation methods: The need for novel single-well solutions. Energy 160, 54–63.

Ghaffaripour, O., Esgandani, G.A., Khoshghalb, A., Shahbodaghkhan, B., 2019. Fully coupled elastoplastic hydro-mechanical analysis of unsaturated porous media using a meshfree method. Int. J. Numer. Anal. Meth. Geomech. 43, 1919–1955. https://doi.org/10.1002/nag.2931.

Ghasemi-Fare, O., Basu, P., 2016. Thermally-induced pore pressure fluctuations around a geothermal pile in sand. Geo-Chicago 2016, 176–184.

Ghasemi-Fare, O., Basu, P., 2018. Influences of ground saturation and thermal boundary condition on energy harvesting using geothermal piles. Energy Build. 165, 340–351.

Ghasemi-Fare, O., Basu, P., 2019. Coupling heat and buoyant fluid flow for thermal performance assessment of geothermal piles. Comput. Geotech. 116, 103211.

Gibb, F.G., 2000. A new scheme for the very deep geological disposal of high-level radioactive waste. J. Geol. Soc. 157, 27–36.

Hartley, J.G., Black, W.Z., 1981. Transient simultaneous heat and mass transfer in moist, unsaturated soils.

Hilgardia, 1943. Thermodynamics of Soil Moisture. 15 (2), 31–298.

Hirschberg, S., Wiemer, S., Burgherr, P., 2014. Energy from the Earth: Deep Geothermal as a Resource for the Future? vdf Hochschulverlag AG.

Johansen, O., 1977. Thermal conductivity of soils. Cold Regions Research and Engineering Lab Hanover NH.

Joshaghani, M., Ghasemi-Fare, O., 2019. A study on thermal consolidation of fine grained soils using modified consolidometer. In: Geo-Congress 2019: Soil Improvement. American Society of Civil Engineers Reston, VA, pp. 148–156.

Khalili, N., Geiser, F., Blight, G.E., 2004. Effective stress in unsaturated soils: review with new evidence. Int. J. Geomech. 4, 115–126. https://doi.org/10.1061/(ASCE)1532-3641(2004)4:2(115).

Khalili, N., Habte, M.A., Zargarbashi, S., 2008. A fully coupled flow deformation model for cyclic analysis of unsaturated soils including hydraulic and mechanical hystereses. Comput. Geotech. 35, 872–889.

Khalili, N., Khabbaz, M.H., Valliappan, S., 2000. An effective stress based numerical model for hydro-mechanical analysis in unsaturated porous media. Comput. Mech. 26, 174–184.

Khalili, N., Loret, B., 2001. An elasto-plastic model for non-isothermal analysis of flow and deformation in unsaturated porous media: formulation. Int. J. Solids Struct. 38, 8305–8330. https://doi.org/10.1016/S0020-7683(01)00081-6.

Khoury, G.A., 2000. Effect of fire on concrete and concrete structures. Prog. Struct. Mat. Eng. 2, 429–447.

Kiamanesh, A.I., 1992. In-situ tuned microwave oil extraction process.

Kodur, V.K.R., Dwaikat, M., 2008. A numerical model for predicting the fire resistance of reinforced concrete beams. Cem. Concr. Compos. 30, 431–443.

Lu, N., Likos, W.J., 2006. Suction stress characteristic curve for unsaturated soil. J. Geotech. Geoenviron. Eng. 132, 131–142.

Nguyen, T.S., Selvadurai, A.P.S., 1995. Coupled thermal-mechanical-hydrological behaviour of sparsely fractured rock: implications for nuclear fuel waste disposal. Int. J. Rock Mech. Min. Sci. Geomech. Abstr. Elsevier 465–479.

Novak, M.D., 2016. Importance of soil heating, liquid water loss, and vapor flow enhancement for evaporation. Water Resour. Res. 52, 8023–8038.

Novak, M.D., 2010. Dynamics of the near-surface evaporation zone and corresponding effects on the surface energy balance of a drying bare soil. Agric. For. Meteorol. 150, 1358–1365.

Olgun, C.G., 2013. Energy piles: background and geotechnical engineering concepts. In: Proceedings of the 16th Annual George F. Sowers Symposium, Atlanta, GA, USA.

Pan, C., Feng, J., Tian, Y., Yu, L., Luo, X., Sheng, G., Fu, J., 2005. Interaction of oil components and clay minerals in reservoir sandstones. Org Geochem. 36, 633–654.

Rees, S.W., Adjali, M.H., Zhou, Z., Davies, M., Thomas, H.R., 2000. Ground heat transfer effects on the thermal performance of earth-contact structures. Renew. Sustain. Energy Rev. 4, 213–265.

Savvidou, C., Booker, J.R., 1989. Consolidation around a heat source buried deep in a porous thermoelastic medium with anisotropic flow properties. Int. J. Numer. Anal. Meth. Geomech. 13, 75–90. https://doi.org/10.1002/nag.1610130107.

Savvidou, C., Booker, J.R., 1988. Consolidation around a spherical heat source with a decaying power output. Comput. Geotech. 5, 227–244.

Selvadurai, A.P.S., Nguyen, T.S., 1997. Scoping analyses of the coupled thermal-hydrological-mechanical behaviour of the rock mass around a nuclear fuel waste repository. Eng. Geol. 47, 379–400.

Senejani, H.H., Ghasemi-Fare, O., Cherati, D.Y., Jafarzadeh, F., 2020. Investigation of thermo-mechanical response of a geothermal pile through a small-scale physical modelling. In: E3S Web of Conferences. EDP Sciences, p. 05016.

Shahbodagh-Khan, B., Khalili, N., Esgandani, G.A., 2015. A numerical model for nonlinear large deformation dynamic analysis of unsaturated porous media including hydraulic hysteresis. Comput. Geotech. 69, 411–423.

Smith, D.W., Booker, J.R., 1993. Green's functions for a fully coupled thermoporoelastic material. Int. J. Numer. Anal. Meth. Geomech. 17, 139–163.

Song, X., Wang, K., Ye, M., 2018. Localized failure in unsaturated soils under non-isothermal conditions. Acta Geotech. 13, 73–85.

Tamizdoust, M.M., Ghasemi-Fare, O., 2020a. A fully coupled thermo-poro-mechanical finite element analysis to predict the thermal pressurization and thermally induced pore fluid flow in soil media. Comput. Geotech. 117, 103250.

Tamizdoust, M.M., Ghasemi-Fare, O., 2020b. Utilization of Nonequilibrium Phase Change Approach to Analyze the Nonisothermal Multiphase Flow in Shallow Subsurface Soils. Water Resour. Res. 56, 10.

Tao, Q., Ghassemi, A., 2010. Poro-thermoelastic borehole stress analysis for determination of the in situ stress and rock strength. Geothermics 39, 250–259.
Teltayev, B.B., Suppes, E.A., 2019. Temperature in pavement and subgrade and its effect on moisture. Case Stud. Therm. Eng. 13, 100363.
Uchaipichat, A., Khalili, N., 2009. Experimental investigation of thermo-hydro-mechanical behaviour of an unsaturated silt. Géotechnique 59, 339–353.
Vahab, M., Khalili, N., 2020. Empirical and Conceptual Challenges in Hydraulic Fracturing with Special Reference to the Inflow. Int. J. Geomech. 20, 04019182.
Wang, D., Lu, L., Zhang, W., Cui, P., 2015. Numerical and analytical analysis of groundwater influence on the pile geothermal heat exchanger with cast-in spiral coils. Appl. Energy 160, 705–714.
Yang, Y., Datcheva, M., Schanz, T., 2016. Axisymmetric analysis of multilayered thermoelastic media with application to a repository for heat-emitting high-level nuclear waste in a geological formation. Geophys. J. Int. 206, 1144–1161.
Yazdani Cherati, Davood, Ghasemi-Fare, Omid, 2021. Practical approaches for implementation of energy piles in Iran based on the lessons learned from the developed countries experiences. Renew. Sustain. Energy Rev. 140 https://doi.org/10.1016/j.rser.2021.110748. https://www.sciencedirect.com/science/article/abs/pii/S1364032121000435.
Zhang, W., Yang, H., Lu, L., Cui, P., Fang, Z., 2014. The research on ring-coil heat transfer models of pile foundation ground heat exchangers in the case of groundwater seepage. Energy Build. 71, 115–128.
Zhang, W., Yang, H., Lu, L., Fang, Z., 2013. The analysis on solid cylindrical heat source model of foundation pile ground heat exchangers with groundwater flow. Energy 55, 417–425.